Journal of Power Sources 516 (2021) 230656

Contents lists available at ScienceDirect

Journal of Power Sources

journal homepage: www.elsevier.com/locate/jpowsour

h-MoO_3/$AlCl_3$-Urea/Al: High performance and low-cost rechargeable Al-ion battery

Paloma Almodóvar [a,*], David Giraldo [a,b], Carlos Díaz-Guerra [c], Julio Ramírez-Castellanos [b], José María González Calbet [b], Joaquín Chacón [a], María Luisa López [b]

[a] Albufera Energy Storage, 28001 Madrid, Spain
[b] Departamento de Química Inorgánica, Facultad de Químicas, Universidad Complutense de Madrid, 28040 Madrid, Spain
[c] Departamento de Física de Materiales, Facultad de Físicas, Universidad Complutense de Madrid, 28040 Madrid, Spain

HIGHLIGHTS

- Al-ion rechargeable battery based on h-MoO_3 and $AlCl_3$/urea has been developed.
- CNTs addition in the electrode leads to high efficiency and stable batteries.
- Compatibility of cheap non-corrosive electrolyte to foster the development of AIBs.

GRAPHICAL ABSTRACT

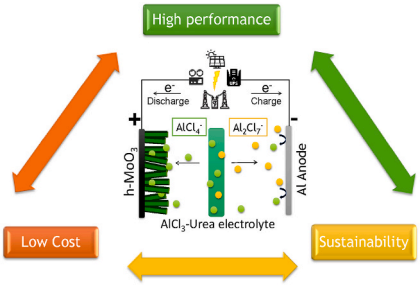

ARTICLE INFO

Keywords:
Al-ion battery
Rechargeable battery
h-MoO_3
Urea

ABSTRACT

A completely functional rechargeable aluminium – ion battery (AIB) operating at room temperature based on hexagonal molybdenum oxide (h-MoO_3) as positive electrode active material and $AlCl_3$-Urea as electrolyte has been developed. This is the first demonstration of the compatibility between a metal oxide and a urea based electrolyte in an AIB. Our battery shows a good electrochemical performance by using this low-cost, eco-friendly, positive electrode - electrolyte system with low corrosion properties. Thanks to an exhaustive study carried out by using different characterization techniques (XRD, micro-Raman, CV), it has been observed that h-MoO_3 is capable of efficiently inserting and de-inserting the redox active species in its crystalline structure by means of controlled diffusion processes. When combined with a suitable amount of carbon nanotubes, the capacitive properties of this material are enhanced, obtaining batteries with a pseudo-capacitive behaviour. This battery reaches specific capacity values ~100 mA h g^{-1} at current densities of 100 mA g^{-1} and ~45 mA h g^{-1} at current densities of 500 mA g^{-1}, always with efficiencies higher than 90%. The obtained results pave the way for the commercialisation of these energy storage devices, providing a promising and simple strategy for the development of high performance, low-cost and non-corrosive AIBs.

* Corresponding author.
E-mail address: palmodov@ucm.es (P. Almodóvar).

https://doi.org/10.1016/j.jpowsour.2021.230656
Received 19 July 2021; Received in revised form 28 September 2021; Accepted 14 October 2021

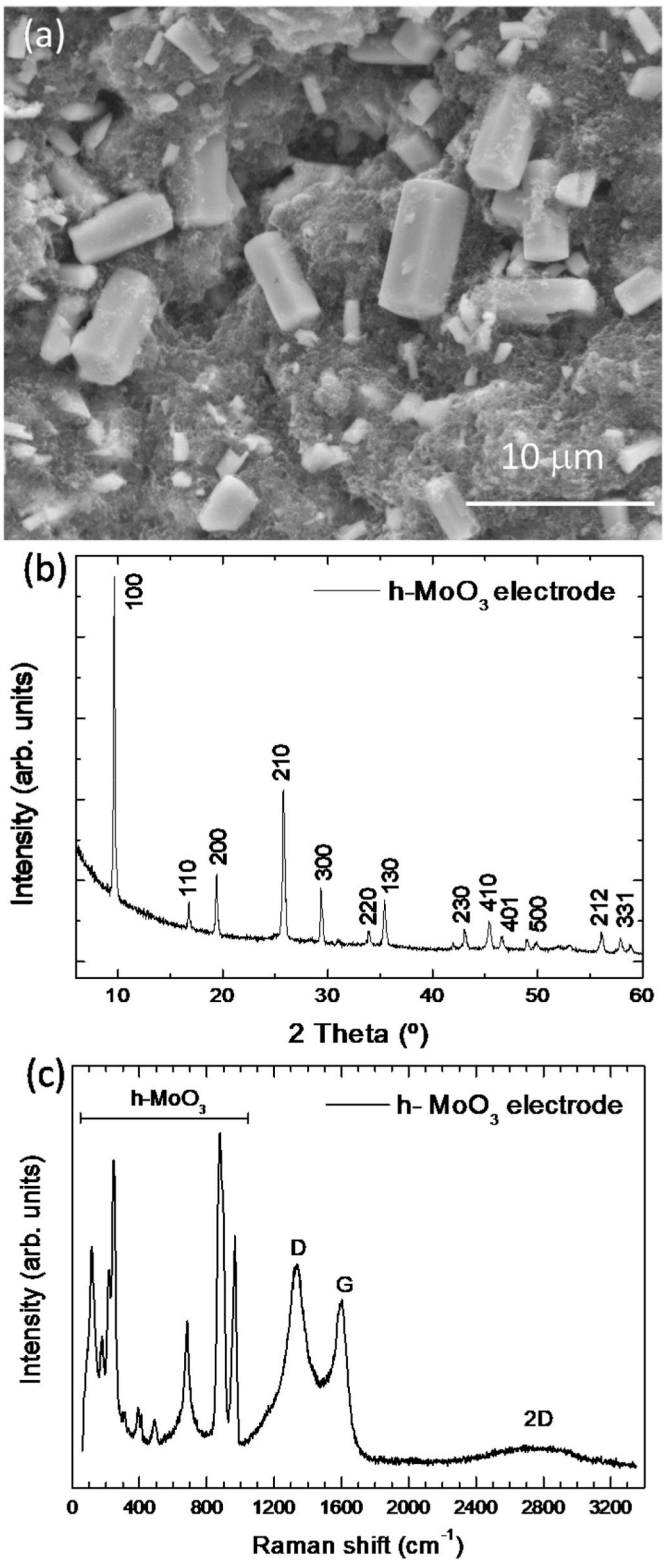

Fig. 1. Morphological and structural characterization of as-prepared h-MoO_3 electrode: (a) SEM image, (b) XRD pattern, (c) Raman spectrum.

1. Introduction

The transition towards the development of renewable energy sources and electric vehicles (EV) has become increasingly important in the last few years. The successful development of energy storage solutions is necessary to overcome the challenges presented by these technologies. New emerging devices such as hybrid supercapacitors, Na-ion, Zn-air, and Al batteries are envisaged as excellent alternatives for stationary applications and EV, as they offer high energy density and greener technology at lower cost [1,2]. In particular, Al based batteries are potential candidates for such applications due to their good electrochemical characteristics and because of socio-economic reasons [3,4]. Within aluminium battery technology, there are several lines of research based on the nature of the electrolyte used, as described by G. A. Elia et al. [5] In particular, one of the most promising lines of research concerns aluminium-ion batteries (AIBs).

AIBs operate with non-aqueous electrolytes, usually ionic liquids, which prevent aluminium corrosion and improve the stability of the electrolyte [6]. Currently, the most widespread electrolyte for these batteries is composed of varying mixtures of 1-ethyl-3-methylimidazolium chloride ([EMIm]) and $AlCl_3$, known as EMIC. Nevertheless, the using of this electrolyte implies that AIBs will have to overcome different obstacles before being introduced on the market. On the one hand, this electrolyte produces redox active chloroaluminate anions ($AlCl_4^-$ and $Al_2Cl_7^-$), with ionic radii of ~6 Å, much larger than Li^+ ions [7,8]. Therefore, the search for cathode materials capable of inserting these species without being pulverised is essential and currently one of the main subjects of research in the field [9–13]. On the other hand, this electrolyte is expensive and highly corrosive, requiring all the components of the battery to be adapted so that they will not be destroyed, which increases the final cost of these devices [14]. Consequently, the search for new electrolytes compatible with this technology is also of paramount importance [15,16].

Molybdenum oxides are versatile semiconductor materials with a wide range of applications, including catalysts, sensors, electronic and energy storage devices [17–19]. Specifically, molybdenum trioxide (MoO_3) is a polymorphic material, which can be found in the α-MoO_3 phase with orthorhombic structure - this being the thermodynamically stable phase - in its two monoclinic phases (β-MoO_3 and MoO_3-II) or in its hexagonal phase (h-MoO_3), which are all metastable [17,20–22]. In recent years, h-MoO_3 has attracted increasing interest, as it has been found to improve some of the properties of the α-MoO_3 phase, such as ionic conductivity, photocatalytic and photochromic activities as well as electrochemical properties [22,23]. This is mainly due to its distinctive crystalline structure, characterised by the presence of tunnels between corner-sharing chains of MoO_6 octahedra along the *c*-axis, which accommodate different ions such as $NH4^+$ or OH^- [19,22]. These kind of crystalline open structures have been previously reported to be very favourable for the intercalation of different ions in other types of batteries such as Li-ion [24] or Zn-ion [25] and even promising results have been obtained in AAIBs [26]. However, they have never been tested so far in AIBs.

Regarding the electrolyte employed, there is a certain experimental evidence that the eutectic liquid formed by mixing $AlCl_3$ and urea gives rise to an electrolyte with the same redox active species as in the case of EMIC, according to the reaction [27,28]:

$$2AlCl_3 + 2\ urea \rightarrow [AlCl_2(urea)_2]^+ + AlCl_4^-$$

$$with\ AlCl_3\ excess:\ AlCl_3 + AlCl_4^- \rightarrow Al_2Cl_7^-$$

This electrolyte has several important advantages. Its price is ~50 times lower than that of EMIC, it is far less corrosive and it is much more eco-friendly [29,30]. However, to date, experiments with this electrolyte have been carried out exclusively on different types of graphite, whereas its compatibility with transition metal oxides has not been tested yet.

In this work we address these two issues by fabricating for the first time an AIB consisting of the combination of h-MoO_3 as positive electrode material and $AlCl_3$-Urea as electrolyte, which can operate at room temperature with high efficiency, according to the schematic drawing represented in Fig. S1.

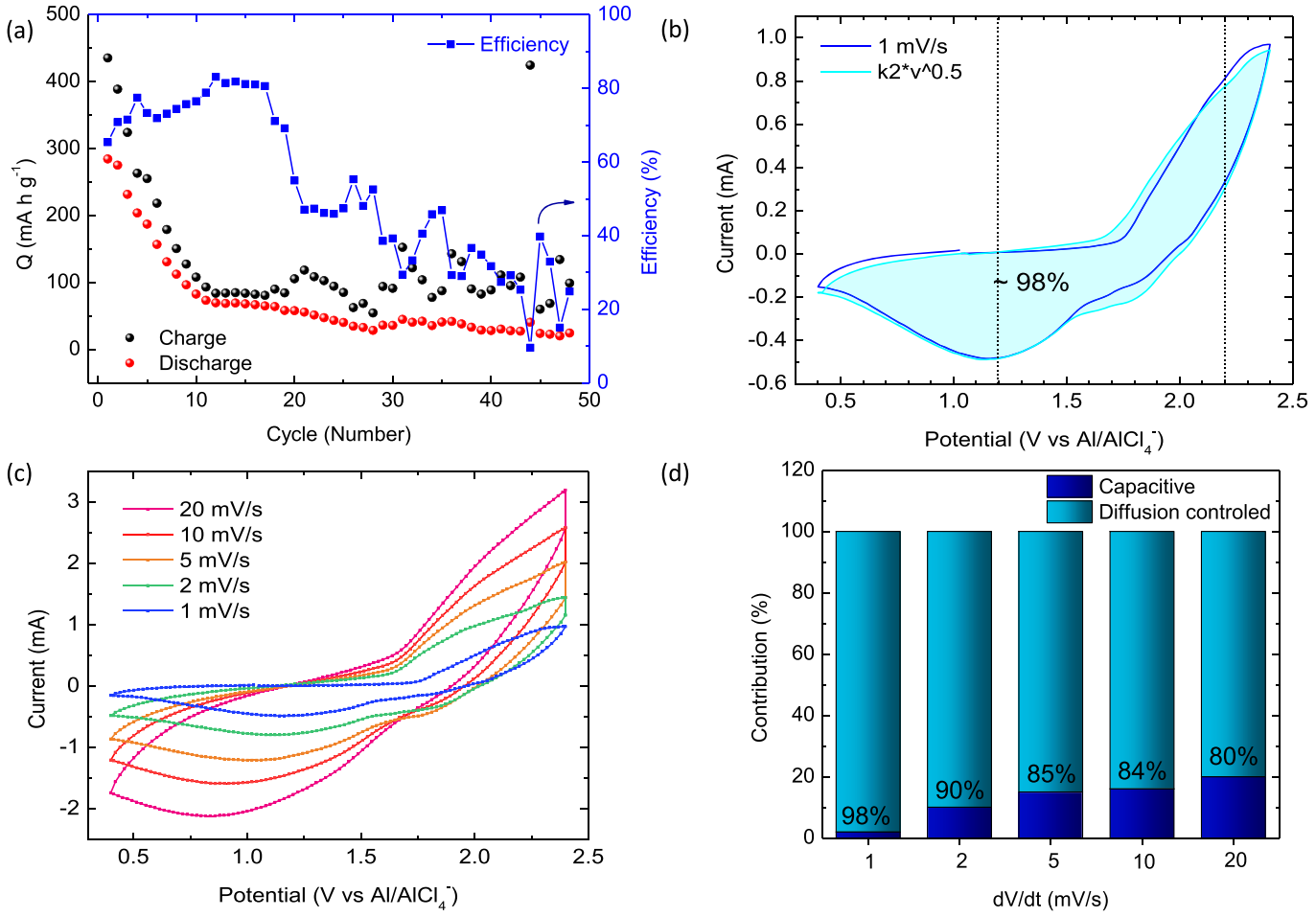

Fig. 2. h-MoO_3 electrochemical characterization: (a) Specific charge-discharge capacity as a function of the cycle number, (b) CV at 1 mV/s with diffusion-controlled contribution, (c) CV at different scan rates and (d) contribution ratio of the capacitive and diffusion-controlled charge versus scan rate.

2. Experimental

2.1. *h-MoO_3 synthesis*

h-MoO_3 was obtained by a low temperature scalable precipitation method described in a previous work [31]. Briefly, 1.22 g of ammonium heptamolybdate tetrahydrate (AHM $(NH_4)_6Mo_7O_{24}{\cdot}4H_2O$, Sigma-Aldrich, 99.98%) were first dissolved in distilled water under magnetic stirring to obtain a 2 M solution. Then, concentrated nitric acid (HNO_3 66%, Panreac) was added dropwise to obtain a white precipitate compound. This solution was heated at 50 °C for 12 h. Finally, the resulting powder was washed and filtered with distilled water for several times and then dried in air at 50 °C for 1 h.

2.2. *Characterization*

X-ray powder diffraction (XRD) patterns were measured at room temperature with a PANanalytical X'PERT POWDER diffractometer using Cu Kα radiation (λ = 1.5418 Å). Scanning electron microscopy (SEM) images and energy dispersive X-ray microanalysis (EDS) elemental mappings were acquired by using a Leica 440 SEM equipped with a Bruker AXS 4010 detector. Micro-Raman measurements were carried out at room temperature in a Horiba Jovin-Ybon LabRAM HR800 on an Olympus BX 41 confocal microscope system with a 633 nm He–Ne laser.

The electrochemical tests were performed at room temperature in 13 mm diameter Swagelok-type cells assembled in an Ar-filled dry box, using graphite paper (Carbon-Foil, Goodfellow) with the same diameter as the cell as current collector (for both negative and positive electrodes). An Al metal foil (99.99%, Nature Alu) of 12 mm diameter was employed as the negative electrode, while a Whatman GF/D borosilicate glass fiber sheet, saturated with a mixture of urea (crystalline urea, Fertiberia) and $AlCl_3$ (99%, Sigma Aldrich) 1:1.5 by mol, was used as electrolyte. The synthesized samples were mixed with carbon SP (Carbon black, Imerys)/carbon nanotubes (CNT-4 Rhenofit, Lanxess) and sodium alginate (Sigma Aldrich) in deionised water with mass proportions 55:25:20. The resultant slurry was coated onto the graphite paper and dried at air overnight. The resulting electrodes had an active material loading of about 1–3 mg. The volume of electrolyte used corresponds to half of that of the active material in ml (0.5–1.5 ml). Charge/discharge cycles as well as CV measurements were performed on an Arbin BT – 2143 Battery Tester potentiostat. EIS data were obtained by applying an AC voltage of 5 mV in the (0.01–100 kHz) frequency range by using a battery tester Biologic BCS – 810.

3. Results and discussion

To study the electrochemical response of h-MoO_3 in AIBs as well as its compatibility with the $AlCl_3$/urea electrolyte, the electrode was initially prepared by mixing the h-MoO_3 material together with carbon black (CB) - which improves electrical conductivity - and with sodium alginate, which has been found to play a beneficial role for the stability of different kind of batteries, as demonstrated in previous studies [9,32]. Fig. 1(a) shows the morphology of the sample before cycling. SEM

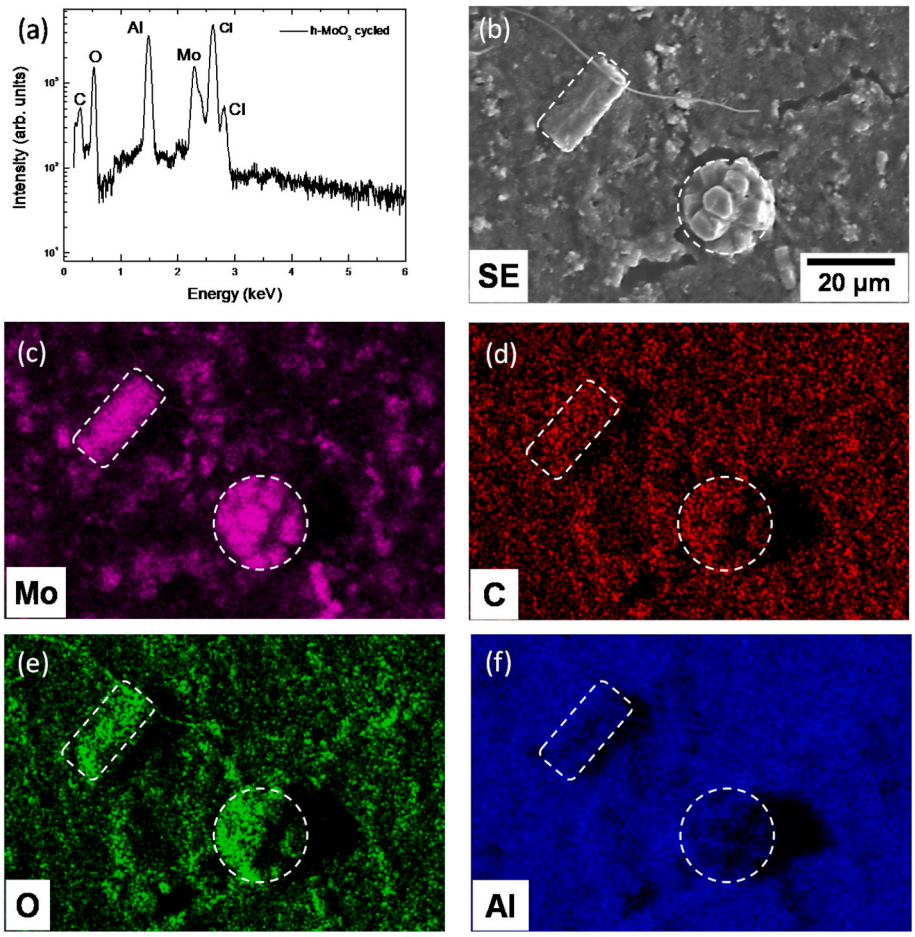

Fig. 3. Ex-situ EDS spectra (a) and EDS compositional mappings of the h-MoO_3 electrode after cycling: (b) SEM image, (c) Mo mapping, (d) C mapping, (e) O mapping, (f) Al mapping.

images show hexagonal microrods with well-defined faces, widths between 1 and 5 μm and lengths up to 6 μm which correspond to h-MoO_3. It can be observed that the micro-rods appear deposited onto CB. SEM-EDS mappings reveal how the Mo and O signals are anti-correlated with that of C, which suggest that these materials do not form a true composite (Fig. S2). Long and short-range structural characterization was respectively carried out by XRD and micro-Raman spectroscopy. Fig. 1(b) show a representative XRD pattern, while a Raman spectrum of the h-MoO_3 electrode can be found in Fig. 1(c). All the diffraction maxima can be indexed according to the JCPDS file 01–078–1027 (lattice constants $a = 10.568$ Å, $c = 3.726$ Å, space group $P6_3/_m$), corresponding to h-MoO_3. Due to the low crystallinity of CB and the low concentration of sodium alginate, XRD patterns only show diffraction maxima related to h-MoO_3. The Raman spectrum show well-defined peaks centred at 118, 133, 175, 220, 250, 312, 396, 413, 493, 689, 886, 901, 914, and 974 cm^{-1}, which can be all attributed to hexagonal MoO_3 [24,31]. A more detailed characterization of this material can be found in our previous works [24,31]. Besides the well-defined Raman peaks corresponding to h-MoO_3, other bands related to CB can be observed as well, such as the D band at 1334 cm^{-1}, the G band at 1598 cm^{-1} and the broad 2D band centred ~2800 cm^{-1} [33]. These results prove that after mixing all the components to obtain the positive electrode material, the h-MoO_3 sample preserves its morphology and crystalline structure.

Once it was verified that the oxide had not been altered by the electrode preparation, the electrochemical characterization of the sample was started. For this purpose, charge and discharge cycles were carried out at a current density of 100 mA g^{-1} at voltages comprised between 0.4 and 2.4 V (voltage limits where the response of this electrolyte has been proved to be stable [28]). In addition, to study the electrochemical kinetics of the sample, cyclic voltammetry (CV) measurements were performed by using scan rates between 1 and 20 mVs^{-1} while keeping the same voltage range. Fig. 2(a) shows the charge/discharge capacity as a function of the number of cycles and the corresponding efficiency.

These results demonstrate the compatibility of the sample with the electrolyte, as it is able to perform several cycles with initial discharge capacities above 300 mA h g^{-1} that end up stabilising around 30 mA h g^{-1}. This initial loss of capacity occurs essentially during the first 10 cycles and can be attributed to two main factors. On the one hand, to the partial decomposition of the electrolyte to give rise to the SEI formation. On the other hand, to the partial transformation that h-MoO_3 might undergo to accommodate its structure for the intercalation of the chloroaluminates [9]. The observed performance is comparable to the results previously obtained with other materials tested as positive electrodes in AIBS [34]. However, these works involve more sophisticated synthesis processes and are conducted with EMIC, which, as explained in the introduction, is a much more corrosive, non-eco-friendly and expensive electrolyte. Nevertheless, a low efficiency and a progressive degradation upon subsequent cycling is observed, which can be mainly attributed to the poor conductivity of h-MoO_3.

Fig. 2(b) shows a CV curve measured at 1 mVs^{-1}. Two redox peaks, corresponding to the insertion and de-insertion of the chloroaluminates in h-MoO_3, appear respectively located at ~2.2 V and ~1.2 V. These voltages agree with the plateaus observed in the charge and discharge

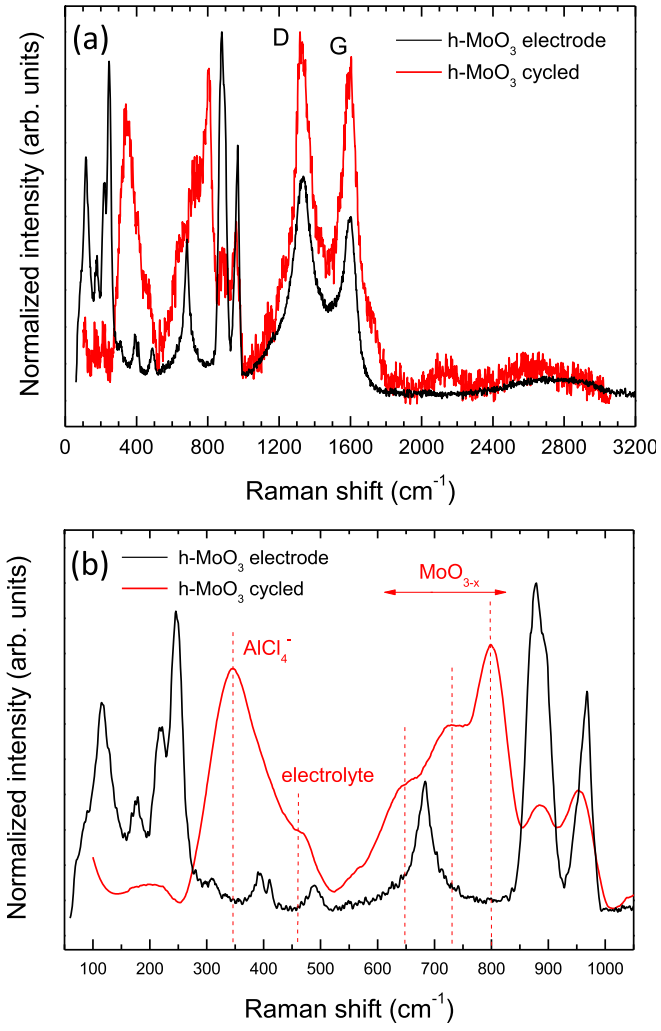

Fig. 4. Ex-situ Raman spectra of a h-MoO_3 electrode cycling: (a) 50–3200 cm^{-1} range (raw data) and (b) 50–1100 cm^{-1} range. The spectrum corresponding to the cycled electrode has been slightly smoothed in this panel by using a FFT filter (cut-off percentage 75) for clarity reasons.

curves (Fig. S3). As shown in Fig. 2(c), the amplitude of these peaks increases with scan rate. To analyse this behaviour in depth and discern whether the nature of the charging and discharging processes correspond to diffusion-controlled or capacitive processes, the following equation was taken into account [35]:

$$i = a\ v^{b}$$

Where current is represented by *i*, the scan rate by *v* and *a* and *b* are variable parameters. Typically, the *b* value is equal to 1 for non-diffusion-controlled-surface capacitive behaviour (supercapacitor behaviour) and equal to 0.5 for diffusion-controlled redox reactions (battery behaviour). Since most materials do not show a unique contribution, this equation can be reformulated as [36]:

$$i(V) = k_1\ v + k_2\ v^{0.5}$$

or, alternatively,

$$i(V) = k_1 v + k_2 v^{0.5}$$

where k_1 and k_2 are adjustable parameters respectively determined from the slope and y-axis intercept of the plots between $i(V)\ v^{-0.5}$ and $v^{0.5}$. In this way, we can find out each type of contribution fraction at different

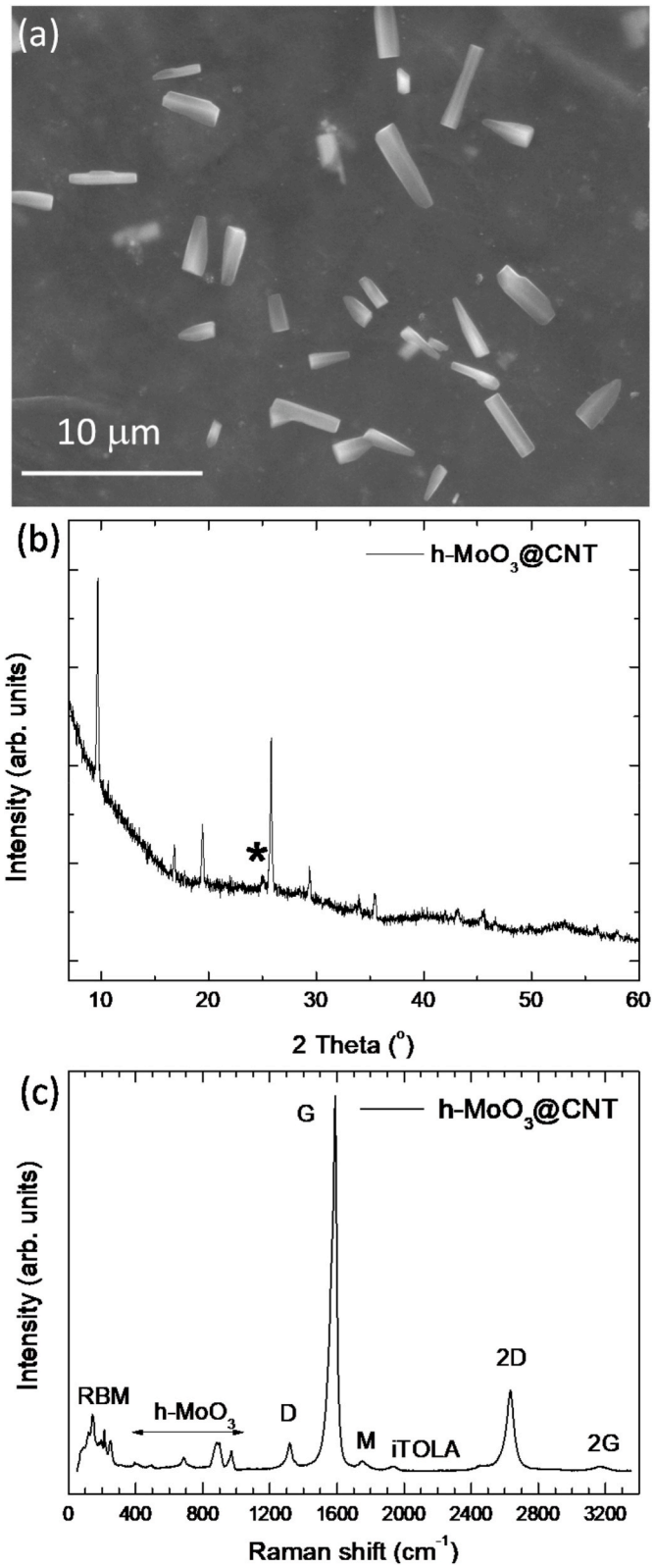

Fig. 5. Morphological and structural characterization of h-MoO_3@CNT. (a) SEM image, (b) XRD pattern (* corresponds to CNTs signal), (c) Raman spectrum.

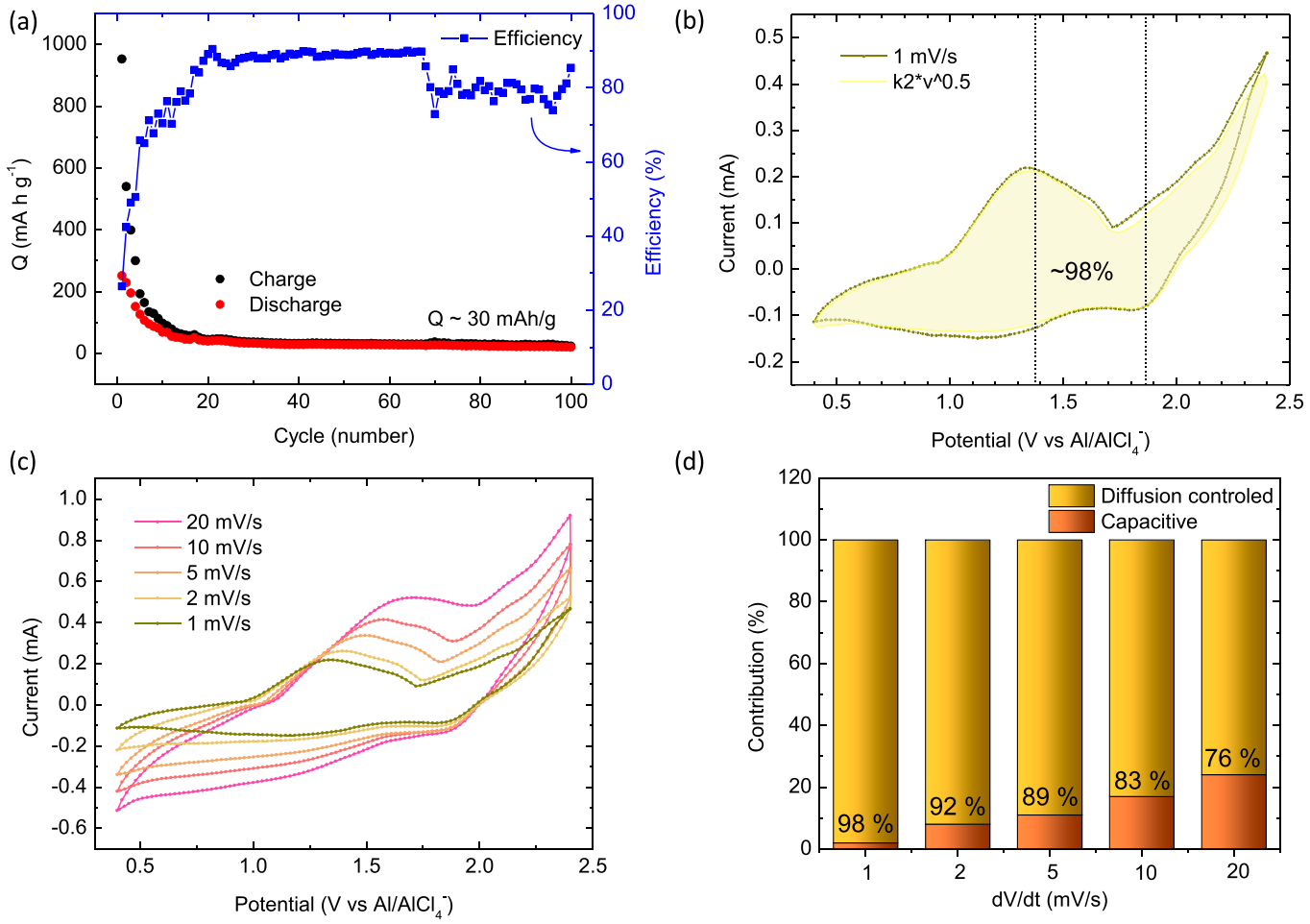

Fig. 6. h-MoO_3x2@CNT electrochemical characterization: (a) Cycling behaviour, (b) CV at 1 mV/s showing diffusion-controlled contribution, (c) CV at different scan rates and (d) contribution ratio of the capacitive and diffusion-controlled charge versus scan rate.

scan rates. The results obtained in the present case are shown in Fig. 2 (d). It can be noticed that the h-MoO_3 sample presents a dominant diffusion-controlled behaviour, even at high scan rates. This result shows that, probably thanks to the tunnel-like arrangement characteristic of h-MoO_3, the active chloroaluminates can find effective diffusion paths along the crystal structure of the material.

To study in detail what happened to the electrode after cycling, *ex-situ* measurements were carried out. Fig. 3 shows a SEM image and the corresponding EDS mappings of a h-MoO_3 electrode after ten consecutive charge and discharge cycles. Besides C, O and Mo, EDS spectra from this sample (Fig. 3(a)) show a noticeable amount of Al and Cl from the electrolyte. The spatial distributions of several elements detected in the spectra are shown in Fig. 3(b)–(f). An h-MoO_3 microrod as well as a flower-like ensemble of microrods have been marked in these mappings for comparison purposes. As expected, Mo and O signals are anti-correlated with that from C. Black areas appearing at the right side of these features are due to a shadow effect related to the position of the EDS detector relative to the sample. Although weaker than in other areas of the imaged sample, Al signal is clearly visible inside the oxide microrods. These results evidence that the hexagonal micro-rods maintain their morphology after cycling and are not pulverised after the insertion and de-insertion processes of the active redox species.

Raman spectra obtained after cycling the sample are shown in Fig. 4. A Raman spectrum of the pristine electrode is also included for comparison purposes. While peaks corresponding to h-MoO_3 are still visible at about 887 and 953 cm^{-1}, these spectra show that h-MoO_3 has been partially transformed into other Mo oxides with lower relative oxygen contents. In fact, three peaks observed at (635–657) cm^{-1}, (708–727) cm^{-1} and (779–799) cm^{-1} can be attributed to Mo_4O_{11} or Mo_8O_{23} [37, 38]. In addition, new spectral features are observed for these cycled materials in the (250–500) cm^{-1} range. Precisely, two peaks centred near (330–346) cm^{-1} and 460 cm^{-1} can be clearly appreciated. The first and more intense of these peaks, previously reported at about 347 cm^{-1} in Raman studies of Al ion batteries with urea-based electrolytes [29, 30], can be assigned to $AlCl_4^-$ ions. The second maximum has also been observed previously in this type of electrolyte, although its origin has not been studied in detail [29]. These new peaks have been marked with red dotted vertical lines in Fig. 4(b).

The possible reduction of h-MoO_3 during active species insertion processes has been suggested in other works concerning Li-ion batteries [24]. Moreover, it has been observed that this metastable phase can partially transit through the above-mentioned intermediate phases while maintaining its hexagonal morphology before transforming into α-MoO_3, which is the thermodynamically stable phase [31]. Hence, taking into account these results as well as the electrochemical mechanisms previously proposed for urea electrolyte-based AIBs [29], we suggest that the following mechanism might account for the h-MoO_3 electrochemical behaviour observed in our batteries: during the first charge, $AlCl_4^-$ ions are intercalated into the channel structure of the oxide and displace some of the NH_4^+ and/or OH^- groups initially located in the mentioned channels. In order to accommodate the chloroaluminate ions, h-MoO_3 partially transforms into other

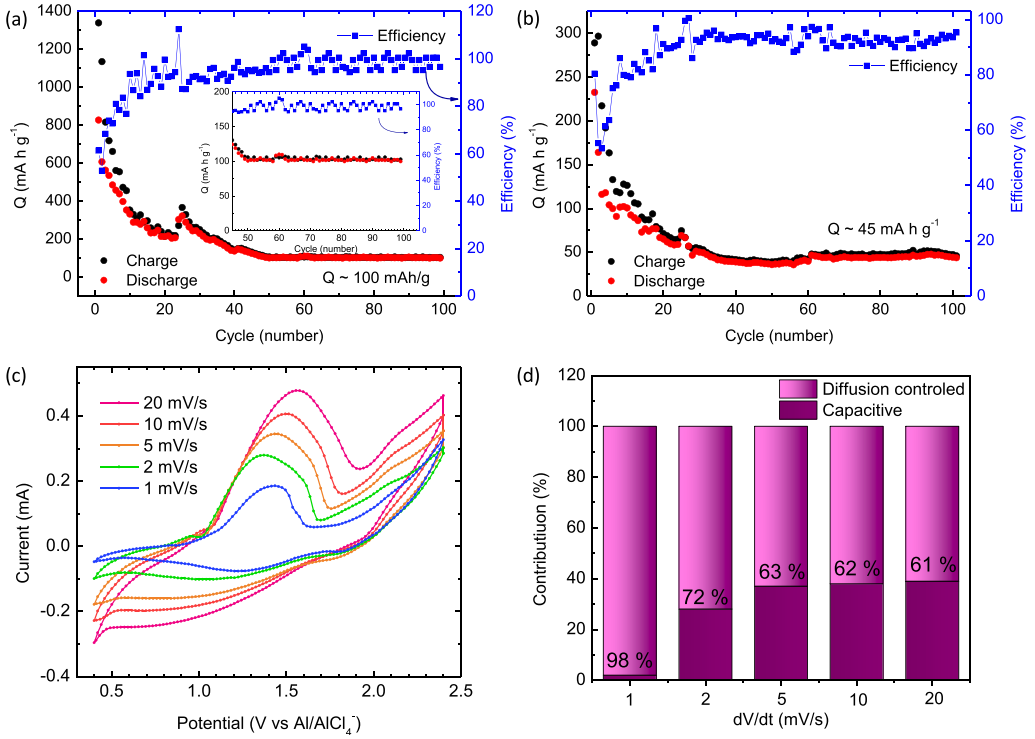

Fig. 7. h-MoO_3@CNT electrochemical characterization: Cycling performance at (a) 100 mA g^{-1} (the inset shows cycles 45–100 to better appreciate the final capacity values achieved) and (b) 500 mA g^{-1}, (c) CV at different scan rates and (d) contribution ratio of the capacitive and diffusion-controlled charge versus scan rate.

mixed-valence Mo (V,VI) oxides, keeping the microrods their original hexagonal morphology. This new structure is stable enough to withstand subsequent charge and discharge processes, during which $AlCl_4^-$ ions are inserted into and de-inserted from the channels. Such assumption agrees with the charge/discharge profiles of this material (Fig. S3), where the first charge curve shows a distinct shape and those corresponding to the subsequent charge processes show a similar appearance. These observations support then the partial transformation of h-MoO_3 during the first charge and its stabilization in the following cycles.

In an attempt to improve the efficiency and stability of our battery, carbon black was replaced by carbon nanotubes (CNTs). It has been reported that the addition of carbon nanotubes to metal oxides significantly improve the electrochemical properties of the latter by providing enhanced conductivity, decreasing substantially the extent of (slow) electron transport through the metal oxide [39]. Moreover, it has been observed that CNTs might form a network which mechanically binds the components of the active material together, providing high strength to the electrode [40]. When characterizing this new electrode, we observed how a pseudo-composite was actually formed between the metal oxide and the CNTs, where h-MoO_3 micro-rods were incorporated to the mentioned network (Fig. 5(a)).

SEM-EDS mappings showing a clear correlation between the spatial distribution of Mo, O and C seem to confirm this observation (Fig. S4). In fact, it has previously been observed that this type of morphology is advantageous for the stability of the electrodes, as it helps h-MoO_3 to resist the volume changes which occur during the charge-discharge reactions [24]. In addition, in both XRD patterns (Fig. 5(b)) and Raman spectra, signals from h-MoO_3 appear together with those of carbon nanotubes (Fig. 5(c)), while no diffraction maxima or Raman peaks associated with other Mo oxides were found. A detailed Raman characterization of the CNTs employed in this work can be found in the supplementary material and Fig. S5.

Before performing the electrochemical characterization of the samples, two types of electrodes were prepared to clearly identify the possible contribution of CNTs: one with a weight ratio of 70:10:20//h-MoO_3:CNTs:Sodium Alginate (h-MoO_3x2@CNT) and the previously characterised sample, with the same weight ratio as the CB electrode, 55:25:20//h-MoO_3:CNTs:Sodium Alginate (h-MoO_3@CNT). Charge/discharge curves were recorded under the same experimental conditions used for the previous sample, i.e., in the (0.4–2.4) V range and at a current density of 100 mA g^{-1}. Fig. 6(a) shows the cycling performance of the h-MoO_3x2@CNT sample. Representative charge/discharge curves can be found in Fig. S6(a). It can be clearly appreciated that the final capacity achieved is close to that obtained previously, ~30 mA h g^{-1}. However, both the efficiency and electrochemical stability increase notably with respect to the initially cycled sample, obtaining efficiency values above 70% over 100 cycles and without observing any capacity decrease once ~15 cycles have been completed. This enhanced electrochemical response may be due to an improvement of the conductivity of the sample and the effective coating of the h-MoO_3 due to the addition of CNTs to the electrode. Regarding the CV performed at 1 mV/s (Fig. 6 (b)), it can be observed how the addition of CNTs gives rise to the appearance of two new redox peaks, ~1.4 V and ~1.9 V. Similar peaks have already been observed in other active carbonaceous species in this type of batteries [29]. However, it should be noted that the cycling performance of CNTs without h-MoO_3 was tested at 100 mA g^{-1} and it was found that the nanotubes alone were not able to perform a single full loading cycle (Fig. S6(b)). This might be due to the type of CNTs employed in this work, as it has been reported that their ability to intercalate the active chloroaluminate species depends strongly on their structure and the accessible active sites they exhibit [41]. By analysing the diffusion-controlled and/or capacitive contributions of the sample through the study of the CVs performed at different rates (Fig. 6(c)–(d)), it was found that the sample still maintains a predominantly diffusive behaviour, whereas at higher scan rates the capacitive behaviour slightly increases thanks to the incorporation of CNTs.

The results obtained for the h-MoO_3@CNT sample show that the capacity obtained at 100 mA g^{-1} (Fig. 7(a)) increases significantly, reaching a value of 100 mA h g^{-1} after 100 cycles (more than three times the previously obtained values). In addition, it can be noticed how the

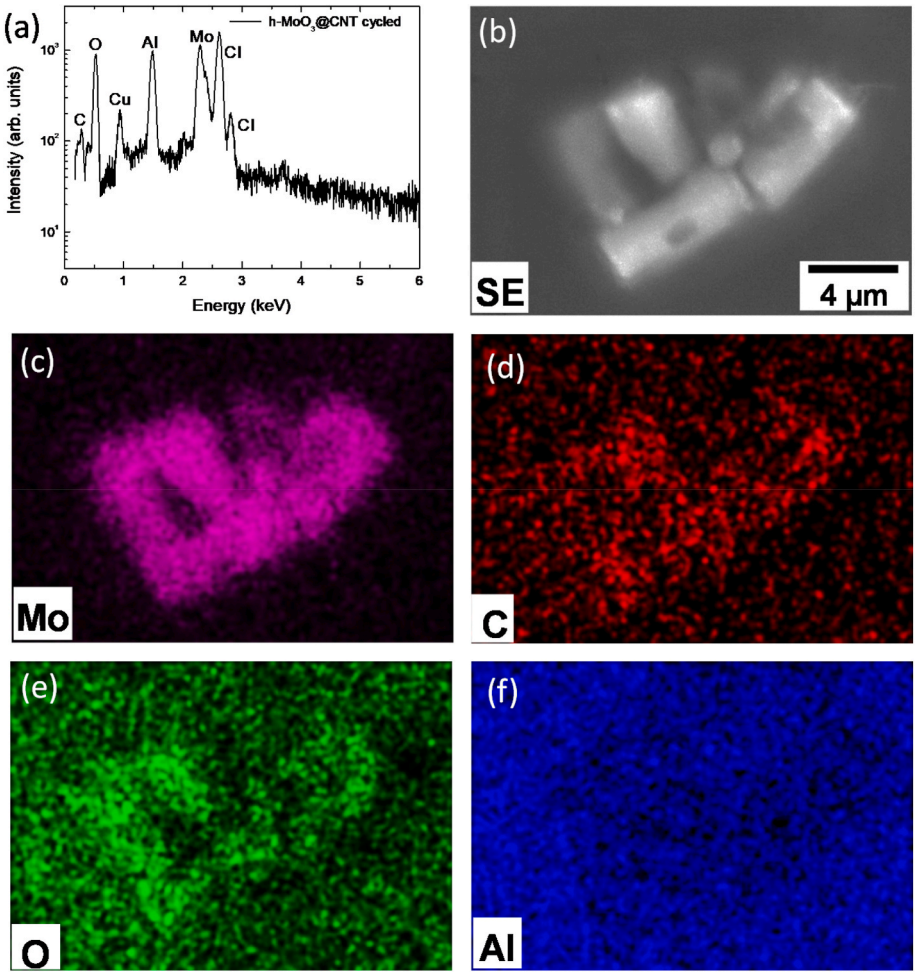

Fig. 8. EDS spectrum (a) and compositional mappings of h-MoO_3@CNT after cycling: (b) SEM image, (c) Mo mapping (d) C mapping, (e) O mapping, (f) Al mapping.

efficiency of the battery is improved again, obtaining values higher than 90% in all cases. Considering the excellent results obtained, the charge/discharge current rate was increased up to 500 mA g^{-1} (Fig. 7(b)). The electrochemical response of the sample was again outstanding, with stabilised capacity values of ~45 mA h g^{-1} and an efficiency of over 90% after 100 cycles. These results represent a very significant improvement with respect to other metal oxides previously tested in AIBs. Not only the capacity values are comparable to or better than those previously reported [9,42,43], but also it is the first time that such results are obtained for a metal oxide using an urea-based electrolyte. Moreover, the electrochemical performance of our batteries is comparable and even better than those AIBs based on urea electrolytes and positive electrodes composed of carbonaceous materials, where similar capacity results have only been achieved for batteries operating at high temperatures (>110 °C) [28–30,44].

When performing the kinetic study of the sample by means of CV curves (Fig. 7(c)–(d)), it can be observed that the intensity of the peaks previously found at ~ 1.4 V and ~1.9 V is enhanced, evidencing the increase of wt% of CNTs in the electrode. These new peaks can be clearly identified in the plateaus of the charge/discharge curves measured at 100 mA g^{-1} (Fig. S7). In addition, it can be observed that at low current densities the behaviour of the sample continues to be almost 100% diffusive. However, as the scan rate increases, the introduction of CNTs causes the sample to behave more pseudo capacitively, this contribution reaching values up to ~40%. This increase in capacitive behaviour is directly related to the improvement of the conductivity of the sample and explains its good electrochemical response when the current density is increased up to 500 mA g^{-1}. The enhanced conductivity of the sample containing CNT was experimentally assessed by EIS measurements shown in Fig. S8.

The results concerning the electrochemical behaviour of the h-MoO_3x2@CNT and h-MoO_3@CNT samples suggest that the addition of CNTs to the electrode promotes the intercalation of the species not only in the bulk of the material but also on the surface. This indicates that our material can present either a high-rate property for the battery or a fast ion insertion/de-insertion when CNTs are added; in other words, it exhibits pseudo-capacitive behaviour [45].

The h-MoO_3@CNT sample was also characterised ex-situ by SEM-EDX after cycling. EDS spectra (Fig. 8(a)) from this sample are quite similar to those measured in the initial h-MoO_3 electrode, since besides C, O and Mo, Al and Cl from the electrolyte are also detected. Cu signal comes from the SEM sample holder. SEM images (Fig. 8(b)) show that the h-MoO_3 microrods can still be observed on the electrode and preserve their hexagonal morphology after cycling. EDS mappings (Fig. 8 (c)–(e)) show Mo and O signals correlate with that from C, which confirms that coating of the Mo oxide microrods by CNTs remains effective during the charging and discharging processes. This effective coating helps to support volume changes caused by the insertion of the active chloroaluminate ions and improves the conductivity of the sample [24,46,47], which is in agreement with the excellent electrochemical response observed. As in the preceding case, Al signal is measurable inside the oxide microrods, which supports the insertion of redox active species. Further evidence of such incorporation was also found by ex-situ spatially resolved Raman spectroscopy measurements (Fig. S9).

4. Conclusions

In summary, we report for the first time a functional Al-ion rechargeable battery based on h-MoO_3 as positive electrode active material and a low-cost, non-corrosive $AlCl_3$/urea electrolyte, which can operate at room temperature. *Ex-situ* SEM-EDS measurements of the cycled electrodes reveal the existence of Al inside the h-MoO_3 microrods, which maintain their morphology after successive charge and discharge cycles. These observations suggest an adequate insertion and de-insertion of the redox active species during the performance of the battery, as supported by micro-Raman spectra showing peaks corresponding to $AlCl_4^-$ ions. Hence, the compatibility between our Mo oxide and the urea-based electrolyte was confirmed and its feasible application in an AIB demonstrated. Moreover, by adding CNTs as active carbon in the electrode, a high efficiency battery, stable over 100 cycles, was built. Precisely, by adjusting the load of CNTs in the electrode, a stable capacity of 100 mA h g^{-1} at a current density of 100 mA g^{-1} and capacity values above 45 mA h g^{-1} at a current density of 500 mA g^{-1} have been achieved. This battery outperforms previously reported AIBs based on carbonaceous materials and urea electrolytes. Therefore, we believe this work provides valuable information for the development of new cathode materials based on metal oxides and its combined use with non-corrosive and cheap electrolytes to foster the development and future commercialisation of rechargeable Al-ion batteries.

Author contributions

Paloma Almodóvar: Conceptualization, Investigation, Data curation, Formal analysis, Writing – Original Draft. **David Giraldo:** Investigation. **Carlos Díaz-Guerra:** Investigation, Data curation, Formal analysis, Writing – Review & Editing. **Julio Ramírez – Castellanos:** Investigation, Writing – Review & Editing. **Jose María González Calbet**: Resources. **Joaquín Chacón:** Supervision, Resources. **María Luisa López:** Supervision, Formal analysis, Writing – Review & Editing.

Declaration of competing interest

The authors declare that they have no known competing financial interests or personal relationships that could have appeared to influence the work reported in this paper.

Acknowledgements

The authors would like to thank Imerys Graphite & Carbon, Fertiberia and Lanxess who kindly provided us with the carbon black, the urea and the CNTs used in this work. The authors are also indebted to UCM XRD CAI centre.

This work has been partially financed by the Spanish Ministry of Economy and Competitiveness (MINECO) under projects MAT2017-84118-C2-2-R and MAT2017-82252-R, as well as by Banco Santander-UCM through project PR87/19–22613.

Appendix A. Supplementary data

Supplementary data to this article can be found online at https://doi.org/10.1016/j.jpowsour.2021.230656.

References

[1] Zachary P. Cano, Dustin Banham, Siyu Ye, Andreas Hintennach, Jun Lu, Michael fowler, Zhongwei chen, batteries and fuel cells for emerging electric vehicle markets, Nat. Energy 3 (2018) 279–289, https://doi.org/10.1038/s41560-018-0108-1.

[2] M. Perrin, Y.M. Saint-Drenan, F. Mattera, P. Malbranche, Lead-acid batteries in stationary applications: competitors and new markets for large penetration of renewable energies, J. Power Sources 144 (2005) 402–410, https://doi.org/10.1016/j.jpowsour.2004.10.026.

[3] N. Jayaprakash, S.K. Das, L.A. Archer, The rechargeable aluminum-ion battery, Chem. Commun. 47 (2011) 12610–12612, https://doi.org/10.1039/c1cc15779e.

[4] T. Leisegang, F. Meutzner, M. Zschornak, W. Münchgesang, R. Schmid, T. Nestler, R.A. Eremin, A.A. Kabanov, V.A. Blatov, D.C. Meyer, The aluminum-ion battery: a sustainable and seminal concept? Front. Chem. 7 (2019) 1–21, https://doi.org/10.3389/fchem.2019.00268.

[5] G.A. Elia, K.V. Kravchyk, M.V. Kovalenko, J. Chacón, A. Holland, R.G.A. Wills, An overview and prospective on Al and Al-ion battery technologies, J. Power Sources 481 (2021), https://doi.org/10.1016/j.jpowsour.2020.228870.

[6] S.K. Das, S. Mahapatra, H. Lahan, Aluminium-ion batteries: developments and challenges, J. Mater. Chem. A. 5 (2017) 6347–6367, https://doi.org/10.1039/c7ta00228a.

[7] D. Lee, G. Lee, Y. Tak, Hypostatic instability of aluminum anode in acidic ionic liquid for aluminum-ion battery, Nanotechnology 29 (2018) 36LT01, https://doi.org/10.1088/1361-6528/aacd7f.

[8] D.Y. Wang, C.Y. Wei, M.C. Lin, C.J. Pan, H.L. Chou, H.A. Chen, M. Gong, Y. Wu, C. Yuan, M. Angell, Y.J. Hsieh, Y.H. Chen, C.Y. Wen, C.W. Chen, B.J. Hwang, C. C. Chen, H. Dai, Advanced rechargeable aluminium ion battery with a high-quality natural graphite cathode, Nat. Commun. 8 (2017), https://doi.org/10.1038/ncomms14283.

[9] P. Almodóvar, D.A. Giraldo, J. Chancón, I. Álvarez-Serrano, M.L. López, δ-MnO_2 nanofibers: a promising cathode material for new aluminum-ion batteries, ChemElectroChem 7 (2020) 2102–2106, https://doi.org/10.1002/celc.202000425.

[10] Z. Hu, K. Zhi, Q. Li, Z. Zhao, H. Liang, X. Liu, J. Huang, C. Zhang, H. Li, X. Guo, Two-dimensionally porous cobalt sulfide nanosheets as a high-performance cathode for aluminum-ion batteries, J. Power Sources 440 (2019) 227147, https://doi.org/10.1016/j.jpowsour.2019.227147.

[11] J. Liu, Z. Li, X. Huo, J. Li, Nanosphere-rod-like Co_3O_4 as high performance cathode material for aluminium ion batteries, J. Power Sources 422 (2019) 49–56, https://doi.org/10.1016/j.jpowsour.2019.03.029.

[12] T. Mori, Y. Orikasa, K. Nakanishi, C. Kezheng, M. Hattori, T. Ohta, Y. Uchimoto, Discharge/charge reaction mechanisms of FeS_2 cathode material for aluminum rechargeable batteries at 55°C, J. Power Sources 313 (2016) 9–14, https://doi.org/10.1016/j.jpowsour.2016.02.062.

[13] X. Zhang, S. Jiao, J. Tu, W.L. Song, X. Xiao, S. Li, M. Wang, H. Lei, D. Tian, H. Chen, D. Fang, Rechargeable ultrahigh-capacity tellurium-aluminum batteries, Energy Environ. Sci. 12 (2019) 1918–1927, https://doi.org/10.1039/c9ee00862d.

[14] Y. Liu, Q. Sun, W. Li, K.R. Adair, J. Li, X. Sun, A comprehensive review on recent progress in aluminum–air batteries, Green Energy Environ 2 (2017) 246–277, https://doi.org/10.1016/j.gee.2017.06.006.

[15] Z. Yu, S. Jiao, S. Li, X. Chen, W.L. Song, T. Teng, J. Tu, H. Sen Chen, G. Zhang, D. N. Fang, Flexible stable solid-state Al-ion batteries, Adv. Funct. Mater. 29 (2019) 1806799, https://doi.org/10.1002/adfm.201806799.

[16] Y. Song, S. Jiao, J. Tu, J. Wang, Y. Liu, H. Jiao, X. Mao, Z. Guo, D.J. Fray, A long-life rechargeable Al ion battery based on molten salts, J. Mater. Chem. A. 5 (2017) 1282–1291, https://doi.org/10.1039/C6TA09829K.

[17] I.A. de Castro, R.S. Datta, J.Z. Ou, A. Castellanos-Gomez, S. Sriram, T. Daeneke, K. Kalantar-zadeh, Molybdenum oxides – from fundamentals to functionality, Adv. Mater. 29 (2017) 1701619, https://doi.org/10.1002/adma.201701619.

[18] P. Jittiarporn, L. Sikong, K. Kooptarnond, W. Taweepreda, Effects of precipitation temperature on the photochromic properties of h-MoO_3, Ceram. Int. 40 (2014) 13487–13495, https://doi.org/10.1016/j.ceramint.2014.05.076.

[19] A. Chithambararaj, A.C. Bose, Investigation on structural, thermal, optical and sensing properties of meta-stable hexagonal MoO_3 nanocrystals of one dimensional structure, Beilstein J. Nanotechnol. 2 (2011) 585–592, https://doi.org/10.3762/bjnano.2.62.

[20] C.V. Krishnan, R. Muñoz-Espí, Q. Li, C. Burger, B. Chu, formation of molybdenum oxide nanostructures controlled by poly(ethylene oxide), Chin. J. Polym. Sci. 27 (2009) 11, https://doi.org/10.1142/S0256767909003613.

[21] E.M. McCarron, J.C. Calabrese, The growth and single crystal structure of a high pressure phase of molybdenum trioxide: MoO_3-II, J. Solid State Chem. 91 (1) (1991) 121–125, https://doi.org/10.1016/0022-4596(91)90064-O.

[22] H.-J. Lunk, H. Hartl, M.A. Hartl, M.J.G. Fait, I.G. Shenderovich, M. Feist, T.A. Frisk, L.L. Daemen, D. Mauder, R. Eckelt, A.A. Gurinov, "Hexagonal molybdenum trioxide"—known for 100 Years and still a fount of new discoveries, Inorg. Chem. 49 (2010) 9400–9408, https://doi.org/10.1021/ic101103g.

[23] A. Chithambararaj, N.S. Sanjini, S. Velmathi, A. Chandra Bose, Preparation of h-MoO_3 and α-MoO_3 nanocrystals: comparative study on photocatalytic degradation of methylene blue under visible light irradiation, Phys. Chem. Chem. Phys. 15 (2013) 14761, https://doi.org/10.1039/c3cp51796a.

[24] P. Almodóvar, M.L. López, J. Ramírez-Castellanos, S. Nappini, E. Magnano, J. M. González-Calbet, C. Díaz-Guerra, Synthesis, characterization and electrochemical assessment of hexagonal molybdenum trioxide (h-MoO_3) microcomposites with graphite, graphene and graphene oxide for lithium ion batteries, Electrochim. Acta 365 (2021) 137355, https://doi.org/10.1016/j.electacta.2020.137355.

[25] T. Xiong, Y. Zhang, Y. Wang, W.S.V. Lee, J. Xue, Hexagonal MoO_3 as a zinc intercalation anode towards zinc metal-free zinc-ion batteries, J. Mater. Chem. A. 8 (2020), https://doi.org/10.1039/d0ta02236e, 9006–9012.

[26] J. Joseph, A.P. O'Mullane, K. Ostrikov, Hexagonal molybdenum trioxide (h-MoO_3) as an electrode material for rechargeable aqueous aluminum-ion batteries, ChemElectroChem 6 (2019) 6002–6008, https://doi.org/10.1002/celc.201901890.

[27] F. Coleman, G. Srinivasan, M. Swadźba-Kwaśny, Liquid coordination complexes formed by the heterolytic cleavage of metal halides, Angew Chem. Int. Ed. Engl. 52 (2013) 12582–12586, https://doi.org/10.1002/anie.201306267.
[28] M. Malik, K.L. Ng, G. Azimi, Physicochemical characterization of $AlCl_3$-urea ionic liquid analogs: speciation, conductivity, and electrochemical stability, Electrochim. Acta 354 (2020) 136708, https://doi.org/10.1016/j.electacta.2020.136708.
[29] M. Angell, C.J. Pan, Y. Rong, C. Yuan, M.C. Lin, B.J. Hwang, H. Dai, High Coulombic efficiency aluminum-ion battery using an $AlCl_3$-urea ionic liquid analog electrolyte, Proc. Natl. Acad. Sci. U.S.A. 114 (2017) 834–839, https://doi.org/10.1073/pnas.1619795114.
[30] H. Jiao, C. Wang, J. Tu, D. Tian, S. Jiao, A rechargeable Al-ion battery: Al/molten $AlCl_3$-urea/graphite, Chem. Commun. 53 (2017) 2331–2334, https://doi.org/10.1039/c6cc09825h.
[31] P. Almodóvar, C. Díaz-Guerra, J. Ramírez-Castellanos, J.M. González-Calbet, In situ local assessment of laser irradiation-induced phase transformations in hexagonal MoO_3 microrods, CrystEngComm 20 (2018) 4954–4961, https://doi.org/10.1039/c8ce00747k.
[32] S.L. Chou, Y. Pan, J.Z. Wang, H.K. Liu, S.X. Dou, Small things make a big difference: binder effects on the performance of Li and Na batteries, Phys. Chem. Chem. Phys. 16 (2014) 20347–20359, https://doi.org/10.1039/c4cp02475c.
[33] M. Pawlyta, J.-N. Rouzaud, S. Duber, Raman microspectroscopy characterization of carbon blacks: spectral analysis and structural information, Carbon 84 (2015) 479–490, https://doi.org/10.1016/j.carbon.2014.12.030.
[34] Z. Hu, H. Zhang, H. Wang, F. Zhang, Q. Li, H. Li, Nonaqueous aluminum ion batteries: recent progress and prospects, ACS Mater. Lett. 2 (2020) 887–904, https://doi.org/10.1021/acsmaterialslett.0c00208.
[35] P. Simon, Y. Gogotsi, B. Dunn, Where do batteries end and supercapacitors begin, Science 343 (2014) 1210–1211, https://doi.org/10.1126/science.1249625.
[36] P. Sirisinudomkit, P. Iamprasertkun, A. Krittayavathananon, T. Pettong, P. Dittanet, M. Sawangphruk, Hybrid energy storage of Ni(OH)2-coated N-doped graphene aerogel//N-doped graphene aerogel for the replacement of NiCd and NiMH batteries, Sci. Rep. 7 (2017) 1124, https://doi.org/10.1038/s41598-017-01191-8.
[37] M. Dieterle, G. Weinberg, G. Mestl, Raman spectroscopy of molybdenum oxides Part I. Structural characterization of oxygen defects in MoO_{3-x} by DR UV/VIS, Raman spectroscopy and X-ray diffraction, Phys. Chem. Chem. Phys. 4 (2002) 812–821, https://doi.org/10.1039/B107012F.
[38] V. Nasretdinova, M. Borov šak, J. Mravlje, P. Šutar, E. Goreshnik, T. Mertelj, D. Mihailovic, Time-resolved reflectivity and Raman studies of the interplay of electronic orders in Mo_8O_{23}, Phys. Rev. B 99 (2019), 085101, https://doi.org/10.1103/PhysRevB.99.085101.
[39] M.G. Bakker, R.M. Frazier, S. Burkett, J.E. Bara, N. Chopra, S. Spear, S. Pan, C. Xu, Perspectives on supercapacitors, pseudocapacitors and batteries, Nanomater. Energy 1 (3) (2012) 136–158, https://doi.org/10.1680/nme.11.00007.
[40] S. Jessl, D. Beesley, S. Engelke, C.J. Valentine, J.C. Stallard, N. Fleck, S. Ahmad, M. T. Cole, M. De Volder, Carbon nanotube conductive additives for improved electrical and mechanical properties of flexible battery electrodes, Mater. Sci. Eng. 735 (2018) 269–274, https://doi.org/10.1016/j.msea.2018.08.033.
[41] E. Zhang, J. Wang, B. Wang, X. Yu, H. Yang, B. Lu, Unzipped carbon nanotubes for aluminum battery, Energy Storage Mater 23 (2019) 72–78, https://doi.org/10.1016/j.ensm.2019.05.030.
[42] M. Vanitha, I. Made Joni, B.M. Wibawa, C. Panatarani, Metal oxides, metal sulphides and hybrid cathode materials for aluminium ion batteries - a mini review, IOP Conf. Ser. Mater. Sci. Eng. 550 (2019), 012003, https://doi.org/10.1088/1757-899X/550/1/012003.
[43] W. Wang, B. Jiang, W. Xiong, H. Sun, Z. Lin, L. Hu, J. Tu, J. Hou, H. Zhu, S. Jiao, A new cathode material for super-valent battery based on aluminium ion intercalation and deintercalation, Sci. Rep. 3 (2013) 3383, https://doi.org/10.1038/srep03383.
[44] C. Wang, J. Li, H. Jiao, J. Tu, S. Jiao, The electrochemical behavior of an aluminum alloy anode for rechargeable Al-ion batteries using an $AlCl_3$-urea liquid electrolyte, RSC Adv. 7 (2017) 32288–32293, https://doi.org/10.1039/c7ra05860h.
[45] J. Li, J. Huang, J. Li, L. Cao, H. Qi, Y. Cheng, Q. Xi, H. Dang, Improved Li-ion diffusion process in TiO_2/rGO anode for lithium-ion battery, J. Alloys Compd. 727 (2017) 998–1005, https://doi.org/10.1016/j.jallcom.2017.08.121.
[46] D.N. Sangeetha, D. Krishna Bhat, M. Selvakumar, h-MoO_3/Activated carbon nanocomposites for electrochemical applications, Ionics 25 (2019) 607–616, https://doi.org/10.1007/s11581-018-2684-2.
[47] K. Zhou, W. Zhou, X. Liu, Y. Sang, S. Ji, W. Li, J. Lu, L. Li, W. Niu, H. Liu, S. Chen, Ultrathin MoO_3 nanocrystalsself-assembled on graphene nanosheets via oxygen bonding as supercapacitor electrodes of high capacitance and long cycle life, Nano Energy 12 (2015) 510–520, https://doi.org/10.1016/j.nanoen.2015.01.017.